Journal of Cellular Physiology

Activated ERK/FOXM1 Pathway by Low-Power Laser Irradiation Inhibits UVB-Induced Senescence Through Down-Regulating p21 Expression

QINGZHOU LING, CHENGBO MENG, QUN CHEN, AND DA XING*

MOE Key Laboratory of Laser Life Science & Institute of Laser Life Science, College of Biophotonics, South China Normal University, Guangzhou, China

Cellular senescence is a growth-arrest program that limits cell proliferation. Low-power laser irradiation (LPLI) has been demonstrated to promote cell proliferation. However, whether LPLI can inhibit cellular senescence remains unknown. In the present study, to investigate the functional role of LPLI against skin aging, we used ultraviolet radiation b (UVB) to induce cell senescence. We first report that LPLI can delay UVB-induced cell senescence. The senescence-associated β-galactosidase (SA-β-Gal) activity and p21 expression, hallmarks of senescent cells, were decreased in the Forkhead box transcription factor FOXM1-dependent manner under treatment with LPLI. The effect of LPLI was further enhanced with an overexpression of FOXM1, and abolished when FOXM1 was knockdown with short hairpin RNA (shRNA). Furthermore, LPLI activated the extracellular regulated protein kinases (ERK) that was upstream of FOXM1. This led to FOXM1 phosphorylation and nuclear translocation. Nuclear translocation enhanced FOXM1 transcriptional activity and promoted its downstream target gene *c-Myc* expression that could inhibit p21 expression. These findings highlight the protective effects of ERK/FOXM1 pathway against UVB-induced cell senescence, suggesting a potential protecting strategy for treating skin aging by LPLI.

J. Cell. Physiol. 229: 108–116, 2014.

Senescent cells differ from other non-dividing (quiescent, terminally differentiated) cells. Hallmarks of senescent cells include an essentially irreversible growth arrest, expression of SA-β-Gal, and p16INK4a (Collado and Serrano, 2005; Ha et al., 2008; Demidenko et al., 2009; Rodier and Campisi, 2011). Skin aging has fascinated worldwide researchers for decades because of its social impact. There are two main processes that can induce skin aging: intrinsic and extrinsic. Evidence shows that both intrinsic and extrinsic aging of the skin are probably driven by similar biological, biochemical, and molecular mechanisms (Rittie and Fisher, 2002). Extrinsic aging, also called photoaging, is mainly due to UV-induced damage of the dermal connective tissue of the skin, resulting in alterations of the dermal extracellular matrix (Wlaschek et al., 2003; Oh et al., 2006). UVB (290–320 nm) is an inherent component of sunlight that can penetrate the epidermis to reach the upper dermis composed mainly of fibroblasts and extracellular matrix (Rosette and Karin, 1996). It interacts with cellular chromatophores and results in DNA damage and activation of signaling pathways related to growth, differentiation, senescence, and connective tissue degradation (Helenius et al., 1999; Kang et al., 2011), such as the activation of the p53-dependent damage response (Campisi, 2005; Lombard et al., 2005; Hill et al., 2008). Morever, the transcription of p53-dependent genes, including that encoding p21, induces cell senescence (Campisi, 2005; Collado and Serrano, 2005; Lombard et al., 2005). p21 is a cyclin-dependent kinase inhibitors (CDKIs) and a crucial mediator of p53-dependent senescence (Brown et al., 1997; Campisi and d'Adda di Fagagna, 2007; Ha et al., 2008; Demidenko et al., 2009). Therefore, inhibition of p21 expression perhaps provides a potential strategy against skin aging-induced by UVB.

FoxM1 is a transcription factor of the Forkhead family. There are three isoforms of FoxM1 (FoxM1a, FoxM1b, and FoxM1c) (Ye et al., 1997; Kaestner et al., 2000; Park et al., 2008a), but only FoxM1b and FoxM1c exhibit transactivation activity (Ye et al., 1997; Leung et al., 2001; Ma et al., 2005). Previous studies demonstrate that FoxM1c is the predominant form expressed in various primary and secondary cell lines (e.g., human BJ1 and mouse NIH3T3 cells) and neonatal tissues rich in mitotically active cells (Yao et al., 1997; Teh et al., 2002; Ma et al., 2005). FoxM1 is expressed in proliferating cells (Korver et al., 1997; Laoukili et al., 2005; Wang et al., 2005). Its expression is initiated just before entry into S phase and peaks at the G2/M phase of the cell cycle (Korver et al., 1997; Leung et al., 2001). FoxM1 depletion in

Conflict of Interest: The authors declare that there is no duality of interest associated with this manuscript.

Contract grant sponsor: The National Basic Research Program of China;
Contract grant numbers: 2011CB910402, 2010CB732602.
Contract grant sponsor: The Program for Changjiang Scholars and Innovative Research Team in University;
Contract grant number: IRT0829.
Contract grant sponsor: The National Natural Science Foundation of China;
Contract grant number: 81101741.

*Correspondence to: Da Xing, MOE Key Laboratory of Laser Life Science & Institute of Laser Life Science, College of Biophotonics, South China Normal University, Guangzhou 510631, China.
E-mail: xingda@scnu.edu.cn

Manuscript Received 15 April 2013
Manuscript Accepted 20 June 2013

Accepted manuscript online in Wiley Online Library (wileyonlinelibrary.com): 26 June 2013.
DOI: 10.1002/jcp.24425

mice and cell lines results in cell cycle defects and chromosomal instability (Laoukili et al., 2005; Wonsey and Follettie, 2005; Li et al., 2008). More importantly, FoxM1$^{-/-}$ MEFs show increased expression of p19Arf and SA-β-Gal that are typical markers of senescent cells (Dimri et al., 1995; Wang et al., 2005; Wu et al., 2007).

Low-energy laser irradiation (LELI) or low level laser irradiation (LLLI) is the use of light in the red, to near infrared, with very low intensity, that induces non-thermo-related biological events (Gavish et al., 2004). It has been employed in a variety of clinical treatments. Light-mediated reaction to LPLI is referred to as biostimulation (Yu et al., 2003). Previous studies have found that LPLI promotes several cellular processes including cell proliferation (Shefer et al., 2001, 2002; Gao et al., 2006; Zhang et al., 2008, 2009) and anti-apoptosis (Zhang et al., 2010b, 2012), promotes collagen synthesis (Gavish et al., 2006), stimulates growth factors release (Saygun et al., 2008), and upregulates cell cycle regulatory protein expression (Shefer et al., 2002; Taniguchi et al., 2009). To date, the role of LPLI against UVB-induced cell senescence and whether FOXM1 can be activated under LPLI have not been investigated.

In the present study, we show that LPLI promoted FOXM1 nuclear translocation in an ERK-dependent manner, enhanced the transactivation of c-Myc, and ultimately resulted in inhibiting UVB-induced p21 expression. The results suggest that LPLI can inhibit UVB-induced cell senescence through ERK/FOXM1 pathway.

Materials and Methods

Materials

Lipofectamine^{TM} 2000 was purchased from Invitrogen (Carlsbad, CA). Hydroxyurea (HU) was purchased from Sigma–Aldrich (St. Louis, MO), HU stock solution of 1 mM was prepared in distilled and deionized water, and stored at 4°C. PD98059 (20 μM) was purchased from Santa Cruz Biotechnology (Santa Cruz, CA). Plasmids pcDNA3-HA-FOXM1c and pTER-shFOXM1 were kindly supplied by Dr. K.M.yao (University of HK, Hong Kong). The pYFP-ERK was a gift from Prof. Michiyuki Matsuda (Osaka University, Japan).

Cell culture and cell cycle synchronization

Mouse embryonic fibroblasts Swiss NIH3T3 cells were obtained from Ji Nan University, and cultured in a humidified (5% CO_2, 37°C) incubator in Dulbecco's modified Eagle's medium (DMEM, Life Technologies, Inc., Grand Island, NY), supplemented with 10% fetal bovine serum, penicillin (100 U/ml), and streptomycin (100 μg/ml). NIH3T3 cells were synchronized by serum deprivation/HU double block. After 30 h, cells were washed three times with PBS and replenished with DMEM and 10% FBS.

UV treatment

UV-irradiation was administrated at 5 mJ/cm^2, the source of UVB radiation was a band of four UVB lamps (Tanon Science Technology Co., Ltd., Shanghai, China) equipped with digital controller to regulate UV dosage at a fixed distance of 15 cm from the lamps to the surface of the cell culture plates. The majority of the wavelengths were in the UVB range and the peak emission was recorded at 314 nm. The NIH3T3 cells were treated with doses of UVB ranged from 0 to 10 mJ/cm^2 with two stresses per day for 3 days. After six exposures to UVB, the cells were detected by the corresponding subsequent treatments and methods.

Low-power laser irradiation

NIH3T3 cells were cultured for 24 h after treatment with UVB and then irradiated with He-Ne laser (632.8 nm, 10 mW, 12.74 mW/cm^2, HN-1000, Guangzhou, China) at a fluence of 1.0 J/cm^2. The entire procedure was carried out as previously described (Gao et al., 2006). The cells were treated with EGF (50 ng/ml) as a positive control. PD98059 (20 μM) was added to the culture medium 30 min before LPLI treatment. The entire procedure was carried out at room temperature. Throughout each experiment, the cells were kept either in a complete dark or a very dim environment, except when subjected to the light irradiation, to minimize the ambient light interference.

Senescence-associated β-galactosidase staining (SA-β-Gal staining)

Phosphate-buffered saline-washed cells were fixed for 5 min (room temperature) in 3.7% formaldehyde. After washing with phosphate-buffered saline (PBS), cells were incubated at 37°C for 12 h with fresh SA-β-Gal stain solution (1 mg of X-gal/ml, 5 mM potassium ferrocyanide, 5 mM potassium ferricyanide, 150 mM NaCl, 2 mM $MgCl_2$, 40 mM citric acid in PBS, pH 6.0).

Cell cycle analysis

To determine the cell cycle distribution, 1×10^6 cells were seeded onto a 100 mm dish. After various treatments, cells were trypsinized at indicated time and fixed with 70% ethanol. Subsequently, cells were stained with RNase I and propidium iodide (PI), and flow cytometric analysis was performed using a FACSCanto^{TM} II flow cytometry (Becton Dickinson, Mountain View, CA) with excitation at 488 nm. The data was analyzed using ModiFit LT software (Verity Software House, Maine).

Cell viability assays and cell apoptosis assay

NIH3T3 cells were cultured in 96-well microplates at a density of 5×10^3 cells/well for 24 h. The cells were then divided into five groups and exposed to UVB at fluence of 1, 2.5, 5, 10 mJ/cm^2. The irradiation was performed on monolayer cells. In all cases, control (non-irradiated) cells were kept in the same conditions as the treated cells. Cell viability was assessed with CCK-8 (Dojindo Laboratories, Kumamoto, Japan) according to the manufacturer's instructions. OD450, the absorbance value at 450 nm, was read with a 96-well plate reader (DG5032, Hua dong, Nanjing, China), to determine the viability of the cells.

Quantification of apoptosis by Annexin-V/PI staining was performed (Rocco et al., 2006; Leong et al., 2007; Zhang et al., 2011). Briefly, both floating and attached cells were collected 72 h after UVB treatment. Apoptotic cell death was determined using the BD ApoAlert Annexin-V-FITC Apoptosis Kit (Becton Dickinson, Biosciences) according to the manufacturer's instructions. Flow cytometry was performed on a BD FACSCanto^{TM} II flow cytometer (Becton Dickinson).

Lysis conditions and preparation of cytosolic and nuclear fractions

Cells were lysed for 40 min on ice in lysis buffer (50 mM Tris–HCl pH 8.0, 150 mM NaCl, 1% Triton X-100, and 100 mM PMSF). The lysates were centrifuged at 12,000 rpm for 5 min at 4°C, protein concentrations were determined using Brasford method.

Cells under various treatments as indicated were lysed in low salt lysis buffer (same as the lysis buffer except NaCl was reduced to 10 mM) and centrifuged at 2,500 rpm for 10 min. The supernatants were used as the cytoplasmic fractions. The pellets were resuspended in high salt lysis buffer (same as the lysis buffer except NaCl was increased to 350 mM) and rotated for 60 min at 4°C and centrifuged at 14,000 rpm. The supernatants were used as the nuclear fractions.

Laser scanning confocal microscopy (LSCM)

To image single cells, the confocal laser scanning microscope system (LSM510-ConfoCor2) (Carl Zeiss, Jena, Germany) was used. All images were acquired after laser irradiation with a Plan-Neofluar 40 × /1.3 NA, oil-immersed objective lens. The specific imaging process is as follows. The excitation wavelengths were 514 nm for pYFP-ERK. The emission detection filters were band pass 520–555 nm for pYFP-ERK. To quantify the results, the fluorescence emission intensities (including the background fluorescence) were obtained with Zeiss Rel 3.2 image processing software (Carl Zeiss).

Immunofluorescence (IF)

After various treatments, cells were fixed in 4% paraformaldehyde for 15 min at room temperature and then were washed five times with PBS. Samples were incubated in blocking buffer (10% bovine serum albumin in PBS) for 1 h at room temperature, followed by incubation with anti-FOXM1 antibody at 4°C overnight. Cells were washed five times for 5 min each, after which FITC-conjugated secondary antibodies (Proteintech Group, Chicago) were added for 2 h at room temperature. Nucleus was stained with PI (10 μg/ml). After five additional washes with PBS, slides were mounted and analyzed by confocal microscopy.

RNA extraction and RT-PCR

RNA extraction and RT-PCR was performed as described in previous studies (Ma et al., 2005). RNA from cells were extracted using the TRIzol™ reagent (Life Technologies) according to the manufacturer's instruction. For semi-quantitative RT-PCR analysis to determine the effect of MEK inhibitor (PD98059) inhibition on FOXM1 expression, NIH 3T3 cells were pre-treated with 20 μM PD98059 at 30 min before LPLI treatment. Total RNAs were extracted at different treatments and 0.4 μg of each sample was subjected to reverse transcription using random hexamers to prime cDNA synthesis. cDNA amounts and cycle numbers were optimized to ensure that amplification was within the linear range for quantitative analysis. FOXM1 and GAPDH cDNAs were amplified using the following primers and cycle numbers: mouse FOXM1, 5′-ACCCAAGTGCCA-ATCGCCACTTG-3′ and 5′-GAAGCGGGGCTATTCCTTCACTGG-3′, 30 cycles (368 bp); mouse GAPDH, 5′-AACGACCCCTTCATTGAC-3′ and 5′-TCCACGACATACTCAGCAC-3′, 30 cycles (191 bp). PCR fragments were resolved in 1% (w/v) agarose gels and detected with ethidium bromide (EB).

Antibodies and Western blotting

The antibodies used for Western blotting include antibodies against FOXM1 (Santa Cruz, CA), ERK (Cell Signaling Technology, Inc., Beverly, MA), phosphoERK (Cell Signaling Technology, Inc.), p21 (Santa Cruz), histone-H3 (Santa Cruz), GAPDH (Guangzhou Jetway Biotech Co.,Ltd, China), Phosphoserine (Millipore Corporation, MA), c-Myc (Bioworld Technology, Inc) and β-actin (Cell signaling Technology, Inc.,). Equivalent samples (40–100 μg of protein extract was loaded on each lane) were subjected to SDS-PAGE on 10% or 13% gel. The proteins were then transferred onto nitrocellulose membranes and probed with the indicated antibody, followed by secondary antibodies: goat anti-mouse conjugated to Alexa Fluor 680 or goat anti-rabbit conjugated to IRDyeTM800. Detection was performed using the LI-COR Odyssey Infrared Imaging System (LI-COR, Inc., Lincoln, NE).

Immunoprecipitation (IP) and coimmunoprecipitation (Co-IP)

Cells were extracted in lysis buffer (50 mM Tris–HCl [pH 8.0], 150 mM NaCl, 1% TritonX-100, 100 mM PMSF) supplemented with protease inhibitor cocktail set I for 60 min on ice. After centrifugation, the protein samples were incubated with 50% slurry of protein A-Sepharose (Roche Applied Sciences, Indianapolis, IN) at 4°C overnight, and these mixed samples were centrifuged at 12,000*g* for 30 sec. The supernatant was incubated with the indicated antibody and subsequently with protein A-Sepharose (50% slurry) at 4°C overnight. The 12,000*g* pellets were washed three times. After adding the same volume of Tris-glycine SDS sample buffer to the sample, these samples were boiled to remove Sepharose beads. After centrifugation at 12,000*g* for 1 min, the cells lysates and immunoprecipitates were analyzed by Western blotting.

Statistical analysis

All data represent at least three independent experiments and are expressed as the mean ± SEM. Differences between groups were compared using Student's *t*-tests by *SPSS* software, and significance was accepted at $P < 0.05$.

Results

UVB induces cell senescence

In order to test the appropriate fluence of UVB (1, 2.5, 5, or 10 mJ/cm^2) that caused NIH3T3 cells senescence without cell death, cell viability was determined by CCK-8 assay. As shown in Figure 1A, the cell viability significantly decreased and cytotoxicity was found after exposure to 10.0 mJ/cm^2, but not 5 mJ/cm^2. Similar results were obtained with flow cytometry assay (Fig. 1B and C).

The SA-β-Gal staining has been used to identify the senescent cells (Dimri et al., 1995; Rodier and Campisi, 2011). It was performed to determine the appropriate UVB treatment that could induce cell senescence. We found that UVB induced cell senescence was in a dose-dependent manner (Fig. 1D and E). Without leading to cell death, the dose of UVB used throughout this study was 5 mJ/cm^2.

FOXM1c is essential for LPLI protecting cells from UVB-induced cell senescence

To address whether FOXM1c could slow down the senescence process, NIH3T3 cells were transfected with HA-FOXM1c for 24 h overexpression and then treated by UVB for 72 h with/without LPLI. As shown in Figure 2A, both overexpression of HA-FOXM1c and LPLI treatment alone inhibited UVB-induced cell senescence by SA-β-Gal staining assay. More importantly, overexpression of HA-FOXM1c with LPLI further suppressed the cell senescence (Fig. 2A and B).

To confirm the role of LPLI against UVB-induced cell senescence, Western blotting was used to detect the stimulation of endogenous p21 expression by UVB-treatment which is a dominant protein believed to be a hallmark of senescent cells (Li et al., 2008). We found that LPLI inhibited the expression of p21 about 20% changes compared to UVB-treated cells at 24 h (Fig. 2C). The p21 expression decreased at 36 h was almost the same as control cells, ultimately inhibited UVB-induced cell senescence (Fig. 2C and D).

In order to detect the role of FOXM1, Western blotting was performed to detect the expression of HA-FOXM1c and test the ability of FOXM1-shRNA to inhibit the expression of FOXM1 (Fig. 2E). As shown in Figure 2F and G, HA-FOXM1c overexpression significantly inhibited the expression of p21 and enhanced the effect of LPLI. However, UVB-induced p21 expression increased after knockdown of FOXM1 by shRNA (Fig. 2H and I).

To further investigate the function of FOXM1c in LPLI attenuating UVB-induced cell senescence, DNA analysis by flow cytometry was performed to detect the percentage of

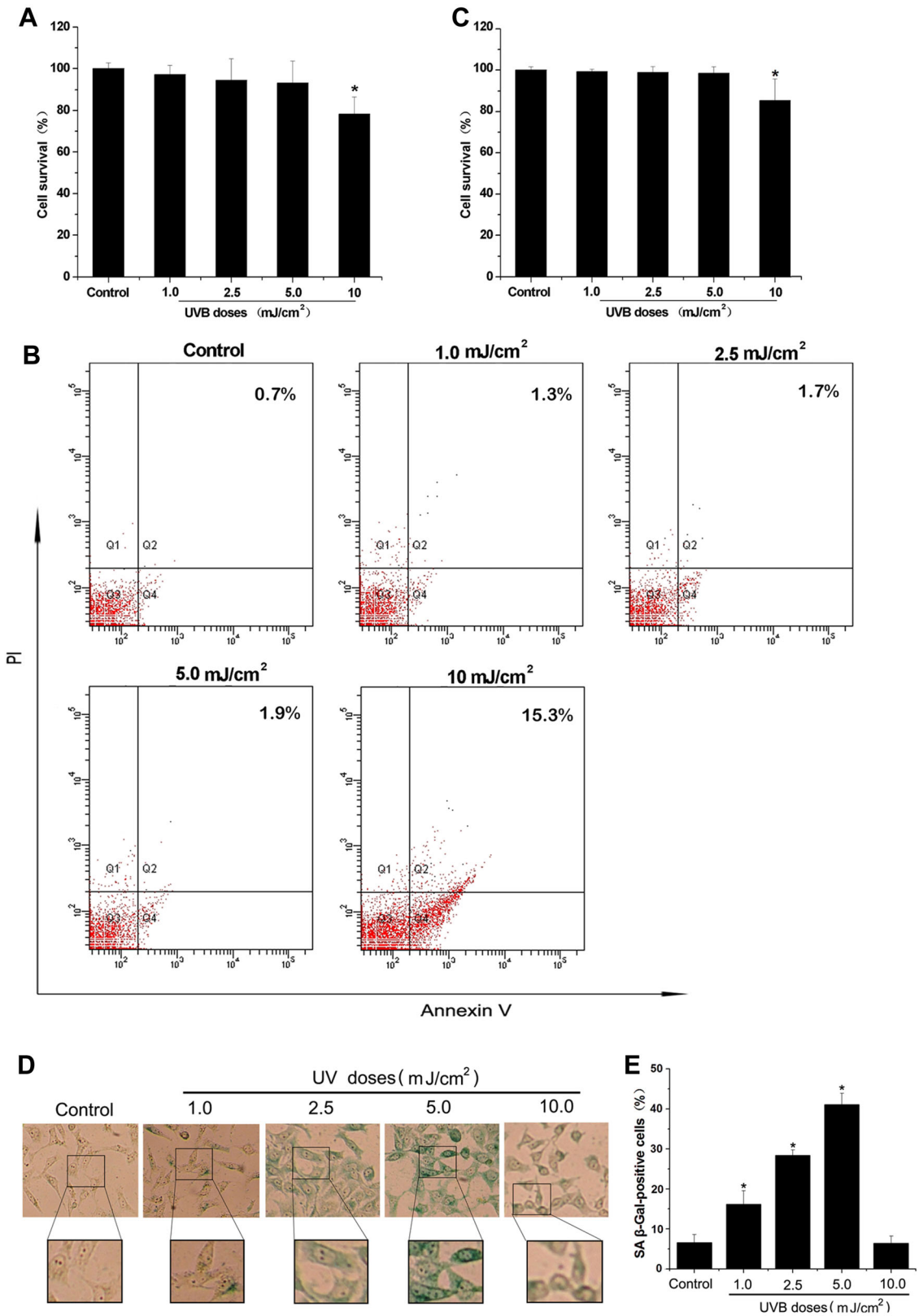

Fig. 1. 5 mJ/cm² UVB induces cell senescence. A: Cytotoxicity was analyzed at 48 h after six exposures to UVB. Doses of UVB ranged from 0 to 10 mJ/cm² with 2 stresses per day for 3 days. Cell viability measured with CCK-8 assay. *$P < 0.05$, significant from the untreated cells. Data represent the mean ± SEM of three independent experiments. B–C: Cell death analysis of treated cells was performed by flow cytometry with Annexin V/PI double staining after six exposures to UVB. B: Numbers refer to the percent Annexin V- and/or PI-positive cells in this representative experiment. C: The percentages of cell viability were used to calculate. *$P < 0.05$, significant from the untreated cells. Data represent the mean ± SEM of three independent experiments. D: NIH3T3 cells were treated with UVB and stained with freshly prepared SA-β-gal staining solution 2 days later. Doses of UVB ranged from 0 to 10 mJ/cm² with two stresses per day for 3 days. E: Quantitative analyses of SA β-Gal-positive cells. Cells in at least four random fields were scored (n ≥ 100 each). *$P < 0.05$.

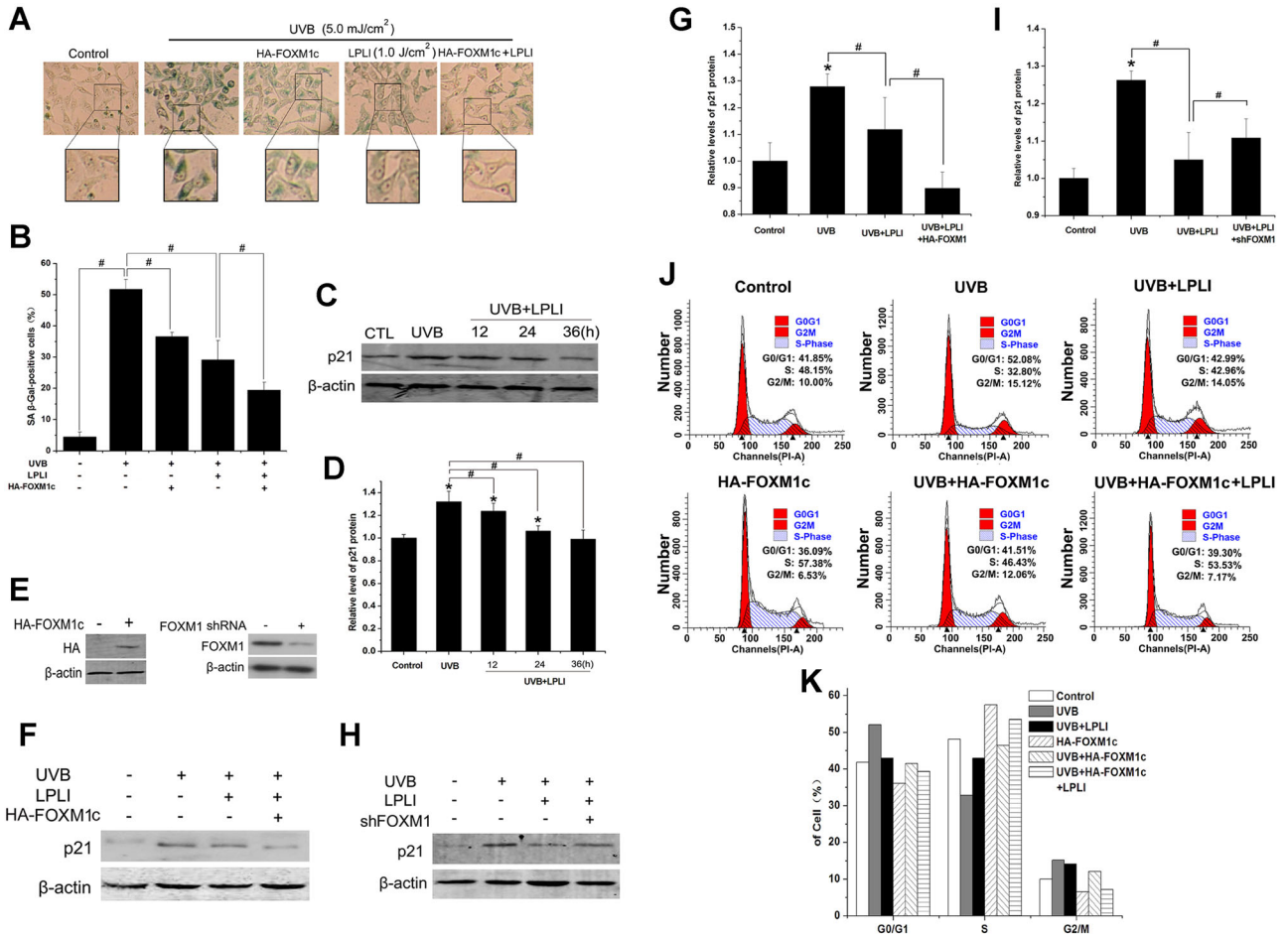

Fig. 2. FOXM1c is essential for LPLI protecting cells from UVB-induced cell senescence. NIH3T3 cells were transfected with HA-FOXM1c or FOXM1 shRNA. A: SA-β-gal staining was performed to analysis cells senescence and the cells were photographed at CCD. NIH3T3 cells were treated with UVB and stained with freshly prepared SA-β-gal staining solution. Similar results were obtained from three independent experiments. B: HA-FOXM1c overexpression further inhibited UVB-induced cell senescence under LPLI. SA-β-gal staining was performed to analysis cells senescence. Quantitative analyses of SA-β-Gal-positive cells. Cells in at least four random fields were scored ($n \geq 100$ each), $^{*}P < 0.05$. C–D: LPLI inhibited the UVB-induced p21 expression. Western blotting was performed to detect p21 expression under different treatments at the indicated times. Similar results were obtained from three independent experiments. Quantitative analysis of p21 levels, $^{*}P < 0.05$, $^{\#}P < 0.05$. E: Western blotting was performed to detect the expression of HA-FOXM1c and test the ability of FOXM1-shRNA to inhibit the expression of FOXM1. F–I: Western blotting was performed to detect the stimulation of endogenous p21 protein expression by UVB treatment plus LPLI with/without HA-FOXM1 (F–G) and FOXM1 shRNA (H–I). Similar results were obtained from three independent experiments. Quantitative analysis of p21 levels, $^{*}P < 0.05$, $^{\#}P < 0.05$. J–K: Flow cytometry analysis the cell cycle of NIH3T3 cells with different treatments. Numbers refer to the percent of cell cycle in this representative experiment (J). Typical cell cycle histograms representing percentage of cells at G1, S, and G2 phases were recorded from three replicate experiments (K).

cells at the G0/G1 phase. We found that overexpression of HA-FOXM1c with/without LPLI treatment significantly decreased the percentage of cells at the G0/G1 phase, suggesting that the protective function was due to an indirect effect of a perturbation in cell cycle progression (Fig. 2J and K).

YFP-ERK translocates from cytoplasm to nucleus and increases its interaction with FOXM1c after LPLI treatment

To determine the role of FOXM1 during LPLI-inhibiting cell senescence, we examined ERK that is upstream of FOXM1 (Ma et al., 2005). ERK localizes in both the nucleus and the cytoplasm under normal physiological conditions (Bonni et al., 1999; Brunet et al., 1999; Burack and Shaw, 2005), and its activity is tightly regulated. YFP-ERK was transfected into NIH3T3 cells to examine its subcellular localization. As shown in Figure 3A, we found that ERK predominantly localized in cytosol in the control cells, while LPLI promoted ERK translocation from cytoplasm to nucleus which was similar to epidermal growth factor (EGF) treatment. Moreover, the effect of LPLI was abolished by PD98059, an inhibitor of MEK (Fig. 3A). These results were further confirmed with a quantitative analysis of nuclear YFP fluorescence emission intensities (Fig. 3B) and detection of the ERK level in nucleus with Western blotting (Fig. 3C). ERK translocation from cytoplasm to nucleus indicated that ERK was activated by LPLI, which was associated with phosphorylation as detected with Western blotting (Fig. 3D).

We have demonstrated ERK is activated by LPLI. To investigate the interaction between ERK and FOXM1c, we examined the ERK-FOXM1c complex by Co-IP. Cells were

treated with (+) or without (−) LPLI and PD98059. As shown in Figure 3E, we found that FOXM1c-ERK complex increased significantly after treatment with LPLI, as well as phosphorylation of FOXM1. The effects were inhibited in the presence of PD98059. Similar results were obtained in HA-FOXM1c transfected cells (Fig. 3F).

LPLI-induced FOXM1 nuclear translocation is in an ERK-dependent manner and enhances the transcriptional activity of FOXM1

FOXM1 expression is initiated before entry into S phase and its level persists during the S phase (Korver et al., 1998; Leung et al., 2001). NIH3T3 cells, synchronized using serum starvation/HU double block, were harvested at various time intervals after release from cell cycle arrest. From 0 to 6 h after release, Western blotting analysis revealed low levels of FOXM1 expression. FOXM1 level increased significantly at 7 h after release, and there was a concomitant mobility shift of the FOXM1 band (Fig. 4A).

To detect FOXM1 subcellular localization under different phase, NIH3T3 cells were similarly synchronized and harvested for immunofluorescence. Cells were stained with propidium iodide (PI) to label the nucleus. Before removal of HU (0 h), low levels of FOXM1 were detected in the nucleus. At 3 and 6 h after release, FOXM1 was still predominately cytoplasmic. Interestingly, there was a dramatic increase in nuclear-expressing cells at 7 h after release (Fig. 4B).

To address whether the subcellular localization of FOXM1 is modulated by LPLI via ERK, synchronized NIH3T3 cells were treated with EGF, PD98059 and LPLI 1-h before the indicated harvest time for immunofluorescence. As shown in Figure 4C, LPLI, which can activate ERK, promoted FOXM1 nuclear translocation at 6 h after release. Without LPLI, FOXM1 did not enter the nucleus. At 7 h after release, FOXM1 translocated to nucleus under normal condition. The nuclear entry was abrogated in the presence of PD98059 (20 μM) with/without LPLI treatment (Fig. 4C). Similar results were obtained in human dermal fibroblasts (HDFs) (Fig. 4D) although nuclear FOXM1 expression levels in HDF cells was not the same as NIH 3T3 cells, likely due to cell-specific variation. These results suggest that FOXM1 nuclear translocation induced by LPLI was in an ERK-dependent manner.

In order to determine the activation of FOXM1 under LPLI, Western blotting and RT-PCR were performed for the expression of FOXM1 at both protein and transcript levels, respectively. c-Myc, the transcriptional target of FOXM1 as described by Wierstra and Alves (2008) and its downstream protein p21 were also investigated. Results show that LPLI increased the expression of FOXM1 at both protein and transcript levels, while PD98059 inhibited the effect of LPLI (Fig. 4E and F). Similar results were obtained from the c-Myc protein expression. Conversely, LPLI significantly suppressed p21 expression and PD98059 neutralized the effect of LPLI

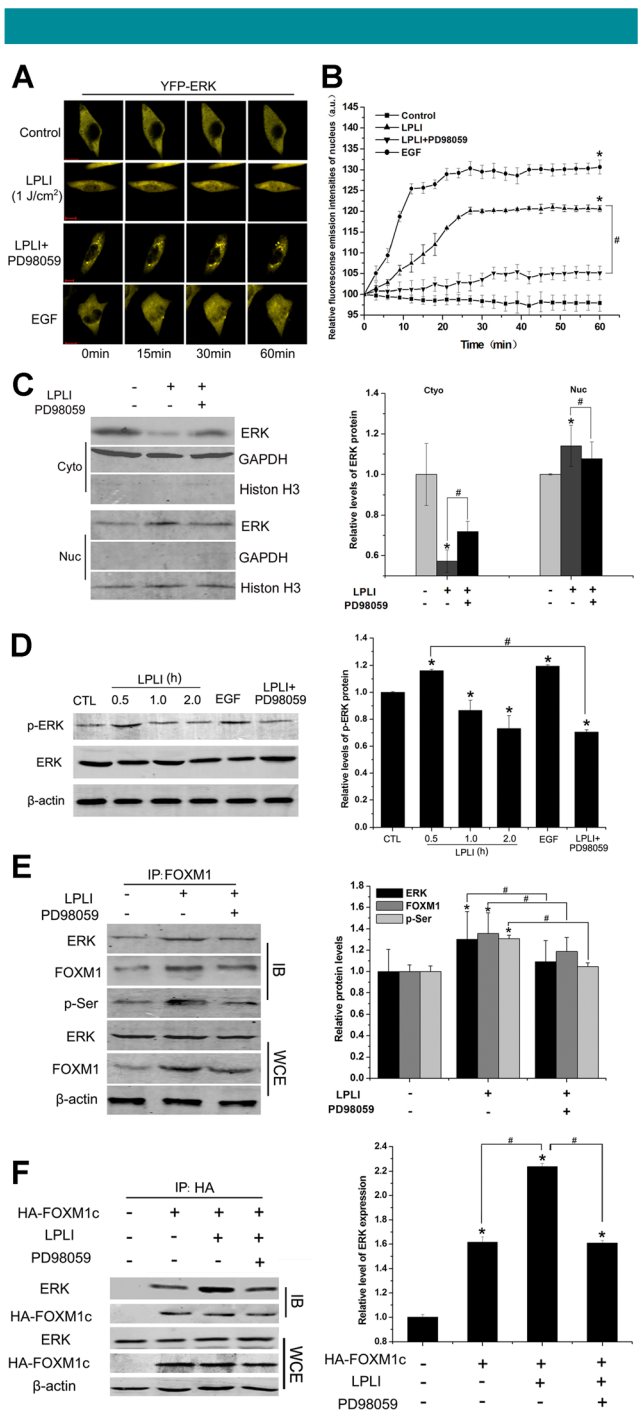

Fig. 3. YFP-ERK translocates from cytoplasm to nucleus and increases its interaction with FOXM1c after LPLI treatment. A: Representative sequential images of NIH3T3 cells expressing YFP-ERK was in response to different treatments; Bar = 10 μm. B: Quantitative analysis of relative YFP-ERK fluorescence emission intensities of nucleus in NIH3T3 cells was subjected to different treatments, $^{*}P < 0.05$, $^{\#}P < 0.05$. C: Western blotting of cytoplamsic and nuclear extracts were designed to examine the level of ERK. Cytoplasmic and nuclear fractions were obtained from the NIH3T3 cells after treatments. Similar results were obtained from three independent experiments. Quantitative analysis of ERK levels, $^{*}P < 0.05$, $^{\#}P < 0.05$. D: Western blotting analysis of NIH3T3 cells under different treatments was performed to detect phosphoration of ERK. Similar results were obtained from three independent experiments. Quantitative analysis of p-ERK levels, $^{*}P < 0.05$, $^{\#}P < 0.05$. E: Co-IP was performed to detect the ERK-FOXM1c complex with or without LPLI/PD98059 treatments. After treatment, Co-IP with an anti-FOXM1 antibody was used to pull down ERK-FOXM1c, Western blotting was performed to detect ERK, FOXM1c, and phosphorylation of FOXM1 in the IP complexes. Similar results were obtained from three independent experiments. Quantitative analysis of ERK-FOXM1c complex levels, $^{*}P < 0.05$, $^{\#}P < 0.05$. F: Co-IP was performed to detect the ERK-HA-FOXM1c complex with or without LPLI/PD98059 treatments. NIH3T3 cells were transfected with HA-FOXM1c. After treatment, Co-IP with an anti-HA antibody was used to pull down ERK-FOXM1c, Western blotting was performed to detect ERK and HA-FOXM1c in the IP complexes. Similar results were obtained from three independent experiments. Quantitative analysis of ERK-HA-FOXM1c complex levels, $^{*}P < 0.05$, $^{\#}P < 0.05$.

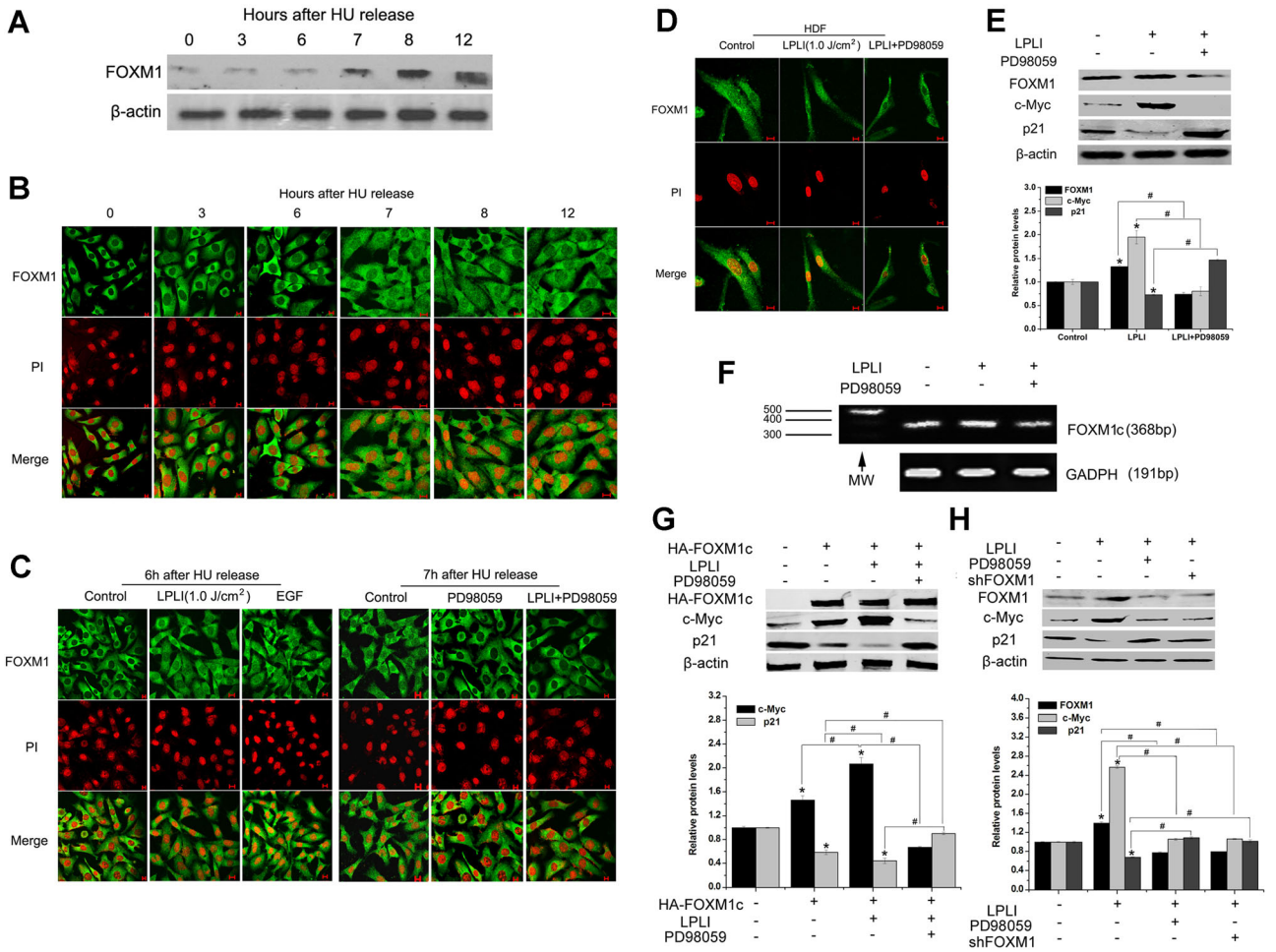

Fig. 4. LPLI induces FOXM1 nuclear translocation is in an ERK-dependent manner and enhances the transcriptional activity of FOXM1. NIH3T3 cells were synchronized at the G1/S boundary by serum starvation/HU double block. A: Cells at different time intervals after HU release were harvested for Western blotting analysis. Progressive mobility shifts of the FOXM1 band were observed at 7 h after release. B: NIH3T3 cells were synchronized by serum starvation/HU double block and fixed at various time points after removal of HU. Immunofluorescence analysis for the localization of endogenous FOXM1 and nucleus was counterstained with PI. Merged images of FOXM1 and nuclear staining were also shown. FOXM1 was predominantly cytoplasmic at 0, 3, and 6 h after release; FOXM1 became mainly in nucleus at 7 h after release. C: Without treatment, FOXM1 was predominantly cytoplasmic at 6 h after release, while LPLI could promote FOXM1 nuclear translocation. Treatment with PD98059 abolished FOXM1 nuclear translocation at 7 h after release with/without LPLI. D: Human dermal fibroblasts (HDFs) cells were synchronized at the G1/S boundary by serum starvation/HU double block. After different treatments, immunofluorescence analysis for the localization of endogenous FOXM1, and nucleus was counterstained with PI. Merged images of FOXM1 and nuclear staining were also shown. Similar results were obtained from three independent experiments. E–F: Western blotting and RT-PCR were performed to evaluate FOXM1 protein expression (E) and its transcript levels (F), respectively. G–H: c-Myc and p21 expression were detected in untransfected (E), HA-FOXM1c-overexpressed (G) or FOXM1-shRNA-transfected (H) cells with/without LPLI/PD98059 treatment. Similar results were obtained from three independent experiments. Quantitative analysis of c-Myc and p21 levels, $^{*}P < 0.05$, $^{\#}P < 0.05$.

(Fig. 4E). Overexpression of HA-FOXM1c promoted the expression of c-Myc with or without LPLI and inhibited the expression of p21 (Fig. 4G), while adding PD98059 or knockdown of FOXM1 decreased c-Myc expression, and enhanced p21 expression even under LPLI (Fig. 4G and H). These suggest that LPLI-induced c-Myc expression and inhibition on p21 were dependent on ERK/FOXM1 pathway.

Discussion

In this study, for the first time, the effect of FOXM1 against UVB-induced cell senescence under LPLI was investigated. Our results show that LPLI reduced SA-β-Gal activity, decreased the expression of p21 protein and G1 phase arrest. These effects were achieved through the activation of the ERK/FOXM1 pathway by LPLI. Overexpression of FOXM1c with/without LPLI attenuated the cell senescence. Inhibition of FOXM1 by shRNA significantly reduced the effect of LPLI on anti-cell senescence induced by UVB. LPLI promoted ERK nuclear translocation, thereby increased FOXM1 accumulation in nucleus and the transactivation of c-Myc, ultimately resulted in inhibition of the p21 expression.

UV radiation is considered to be the most important factor in skin aging, especially in premature aging (Wlaschek et al., 2003). In the present study, cell viability and cell death analysis demonstrated that UVB led cell senescence was in a dose-dependent manner (Fig. 1). Based on this preliminary

study, we developed a model of premature senescence induced with a subcytotoxic UVB dose (5 mJ/cm^2).

LPLI has been shown to increase cell proliferation (Shefer et al., 2001, 2002; Zhang et al., 2009; Huang et al., 2013). Cellular senescence is a growth-arrest program that limits cell proliferation. However, to date, there is no reported investigation of LPLI on protecting against UVB-induced cell senescence. Our results demonstrate that LPLI could protect against UVB-induced cell senescence in NIH3T3 cells. Senescence-associated β-galactosidase (SA-β-Gal) activity and p21 expression were increased after UVB. Under LPLI treatment, both SA-β-Gal positive cells and p21 expression decreased, suggesting that LPLI could delay cell senescence (Fig. 2).

How LPLI delays cell senescence is still unknown. It is well established that FoxM1 is a key cell cycle regulator of both the transition from G1 to S phase and progression to mitosis (Leung et al., 2001; Wang et al., 2002; Laoukili et al., 2005; Wonsey and Follettie, 2005; Park et al., 2008a,b). An accumulation of cell cycle in G0/G1 was observed after UVB treatment. With LPLI treatment, the percentage in G0/G1 phase decreased, while that in the S phase increased. This indicates that LPLI relieved cell cycle arrest induced by UVB (Fig. 2). Furthermore, overexpression of HA-FOXM1c with LPLI significantly decreased the percentage of cells at the G0/G1 phase comparing to that under LPLI alone (Fig. 2), suggesting that the protective function was due to an indirect effect of a perturbation in cell cycle progression through FOXM1. The SA-β-Gal activity and p21 expression were also further decreased when HA-FOXM1c overexpression under LPLI treatment. Knockdown of FOXM1 increased UVB-induced p21 expression (Fig. 2). These results suggest that LPLI delayed UVB-induced cell senescence through FOXM1.

FOXM1 subcellular localization and expression vary in different cell phases. Using synchronized NIH3T3 cells, we show that the FOXM1 expression increased from 7 to 12 h after release from HU. FOXM1 began to translocate to nucleus at 7 h after the release, while LPLI accelerated FOXM1 nuclear translocation at 6 h after the release and there was an associated activation of FOXM1 (Fig. 4). It has been proved that FOXM1 nuclear translocation requires Raf/MEK/MAPK/ERK signaling (Ma et al., 2005). Our results found that FOXM1 nuclear translocation induced by LPLI was abolished when the cells were incubating with the MEK inhibitor PD98059 (Fig. 4), suggesting activation of the MEK/ERK pathway was necessary for stimulating nuclear translocation of FOXM1. The effect of LPLI on MEK/ERK pathway was investigated. The results show that LPLI promoted ERK translocation from cytoplasm to nucleus associated with the phosphorylation of ERK, and PD98059 inhibited this process (Fig. 3).

Previous studies indicate that there are similar results when HDFs and NIH 3T3 cells under the same stimulates such as MEK inhibitor PD98059 and IL-1 suppress basal and TGF-β-induced CTGF mRNA and protein expression (Zhao et al., 2004; Nowinski et al., 2010). Recent studies have demonstrated that *Centella asiatica* extracts regulates HDFs senescence induced by hydrogen peroxide partly through promoting FOXM1 expression (Kim et al., 2011). FoxM1 counteracts oxidative stress-induced NIH 3T3 cells senescence via up-regulating c-Myc expression, resulting in suppressing p21 expression (Li et al., 2008). Reduced c-Myc triggers cell senescence (Guney et al., 2006). Our results show that c-Myc expression increased, while p21 was decreased under LPLI (Fig. 4) and could inhibit cell senescence. The effect of LPLI were inhibited in the presence of PD98059 (Fig. 4). Therefore, there results confirm that LPLI delayed UVB-induced cell senescence through FOXM1/c-Myc/p21 pathway.

In conclusion, our study demonstrates that LPLI realizes its anti-aging effect by activating the ERK/FOXM1/p21 signaling pathway. LPLI phosphorylates ERK, leading to the ERK's cytoplasm-to-nuclear translocation and promotes FOXM1 nuclear translocation. Nuclear localization enhances FOXM1 transcriptional activity and promotes its downstream target gene *c-Myc* expression and inhibits UVB-induced p21 expression, ultimately delays cell senescence. A schematic of the mechanism is summarized in Figure 5.

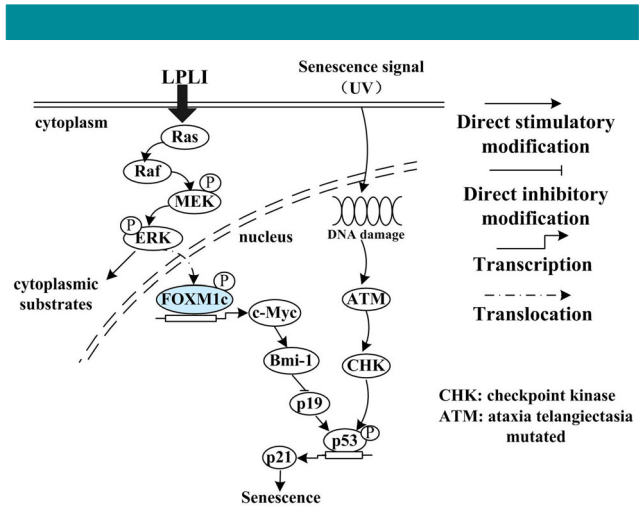

Fig. 5. A model of the signaling pathways for LPLI protecting cell from UVB-induced senescence.

The delineation of the ERK/FOXM1/p21 signaling pathways involved in LPLI inhibiting UVB-induced cell senescence provides an insight into establishing LPLI as a novel approach to against skin aging therapy. FOXM1 protein may be a therapeutic target and LPLI may provide a potential therapeutic strategy for the treatment of photoaging through activating ERK/FOXM1/p21 signaling pathway.

Acknowledgments

This research is supported by the National Basic Research Program of China (2011CB910402; 2010CB732602), the Program for Chang Jiang Scholars and Innovative Research Team in University (IRT0829), and the National Natural Science Foundation of China (30870676; 30870658). We thank Prof. Kwok-Ming Yao in Department of Biochemistry, Faculty of Medicine, the University of Hong Kong for kindly providing the plasmid pcDNA3-HA-FOXM1c, TER-shFOXM1 and Michiyuki Matsuda in Department of Signal Transduction, Research Institute for Microbial Diseases, Osaka University, Japan for kindly providing the plasmid YFP-ERK.

Literature Cited

Bonni A, Brunet A, West AE, Datta SR, Takasu MA, Greenberg ME. 1999. Cell survival promoted by the Ras-MAPK signaling pathway by transcription-dependent and -independent mechanisms. Science 286:1358–1362.

Brown JP, Wei W, Sedivy JM. 1997. Bypass of senescence after disruption of p21CIP1/WAF1 gene in normal diploid human fibroblasts. Science 277:831–834.

Brunet A, Roux D, Lenormand P, Dowd S, Keyse S, Pouyssegur J. 1999. Nuclear translocation of p42/p44 mitogen-activated protein kinase is required for growth factor-induced gene expression and cell cycle entry. EMBO J 18:664–674.

Burack WR, Shaw AS. 2005. Live cell imaging of ERK and MEK: Simple binding equilibrium explains the regulated nucleocytoplasmic distribution of ERK. J Biol Chem 280:3832–3837.

Campisi J. 2005. Senescent cells, tumor suppression, and organismal aging: Good citizens, bad neighbors. Cell 120:513–522.

Campisi J, d'Adda di Fagagna F. 2007. Cellular senescence: When bad things happen to good cells. Nat Rev 8:729–740.

Collado M, Serrano M. 2005. The senescent side of tumor suppression. Cell cycle 4:1722–1724.
Demidenko ZN, Zubova SG, Bukreeva EI, Pospelov VA, Pospelova TV, Blagosklonny MV. 2009. Rapamycin decelerates cellular senescence. Cell cycle 8:1888–1895.
Dimri GP, Lee X, Basile G, Acosta M, Scott G, Roskelley C, Medrano EE, Linskens M, Rubelj I, Pereira-Smith O, Peacocke M. 1995. A biomarker that identifies senescent human cells in culture and in aging skin in vivo. Proc Natl Acad Sci USA 92:9363–9367.
Gao X, Chen T, Xing D, Wang F, Pei Y, Wei X. 2006. Single cell analysis of PKC activation during proliferation and apoptosis induced by laser irradiation. J Cell Physiol 206:441–448.
Gavish L, Asher Y, Becker Y, Kleinman Y. 2004. Low level laser irradiation stimulates mitochondrial membrane potential and disperses subnuclear promyelocytic leukemia protein. Lasers Surg Med 35:369–376.
Gavish L, Perez L, Gertz SD. 2006. Low-level laser irradiation modulates matrix metalloproteinase activity and gene expression in porcine aortic smooth muscle cells. Lasers Surg Med 38:779–786.
Guney I, Wu S, Sedivy JM. 2006. Reduced c-Myc signaling triggers telomere-independent senescence by regulating Bmi-1 and p16(INK4a). Proc Natl Acad Sci USA 103:3645–3650.
Ha L, Merlino G, Sviderskaya EV. 2008. Melanomagenesis: Overcoming the barrier of melanocyte senescence. Cell cycle 7:1944–1948.
Helenius M, Makelainen L, Salminen A. 1999. Attenuation of NF-kappaB signaling response to UVB light during cellular senescence. Exp Cell Res 248:194–202.
Hill R, Bodzak E, Blough MD, Lee PW. 2008. p53 Binding to the p21 promoter is dependent on the nature of DNA damage. Cell cycle 7:2535–2543.
Huang L, Tang Y, Xing D. 2013. Activation of nuclear estrogen receptors induced by low-power laser irradiation via PI3-K/Akt signaling cascade. J Cell Physiol 228:1045–1059.
Kaestner KH, Knochel W, Martinez DE. 2000. Unified nomenclature for the winged helix/forkhead transcription factors. Genes Dev 14:142–146.
Kang ES, Iwata K, Ikami K, Ham SA, Kim HJ, Chang KC, Lee JH, Kim JH, Park SB, Kim JH, Yabe-Nishimura C, Seo HG. 2011. Aldose reductase in keratinocytes attenuates cellular apoptosis and senescence induced by UV radiation. Free Radic Biol Med 50:680–688.
Kim YJ, Cha HJ, Nam KH, Yoon Y, Lee H, An S. 2011. Centella asiatica extracts modulate hydrogen peroxide-induced senescence in human dermal fibroblasts. Exp Dermatol 20:998–1003.
Korver W, Roose J, Clevers H. 1997. The winged-helix transcription factor Trident is expressed in cycling cells. Nucleic Acids Res 25:1715–1719.
Korver W, Schilham MW, Moerer P, van den Hoff MJ, Dam K, Lamers WH, Medema RH, Clevers H. 1998. Uncoupling of S phase and mitosis in cardiomyocytes and hepatocytes lacking the winged-helix transcription factor Trident. Curr Biol 8:1327–1330.
Laoukili J, Kooistra MR, Bras A, Kauw J, Kerkhoven RM, Morrison A, Clevers H, Medema RH. 2005. FoxM1 is required for execution of the mitotic programme and chromosome stability. Nat Cell Biol 7:126–136.
Leong CO, Vidnovic N, DeYoung MP, Sgroi D, Ellisen LW. 2007. The p63/p73 network mediates chemosensitivity to cisplatin in a biologically defined subset of primary breast cancers. J Clin Invest 117:1370–1380.
Leung TW, Lin SS, Tsang AC, Tong CS, Ching JC, Leung WY, Gimlich R, Wong GG, Yao KM. 2001. Over-expression of FoxM1 stimulates cyclin B1 expression. FEBS Lett 507:59–66.
Li SK, Smith DK, Leung WY, Cheung AM, Lam EW, Dimri GP, Yao KM. 2008. FoxM1c counteracts oxidative stress-induced senescence and stimulates Bmi-1 expression. J Biol Chem 283:16545–16553.
Lombard DB, Chua KF, Mostoslavsky R, Franco S, Gostissa M, Alt FW. 2005. DNA repair, genome stability, and aging. Cell 120:497–512.
Ma RY, Tong TH, Cheung AM, Tsang AC, Leung WY, Yao KM. 2005. Raf/MEK/MAPK signaling stimulates the nuclear translocation and transactivating activity of FOXM1c. J Cell Sci 118:795–806.
Nowinski D, Koskela A, Kiwanuka E, Bostrom M, Gerdin B, Ivarsson M. 2010. Inhibition of connective tissue growth factor/CCN2 expression in human dermal fibroblasts by interleukin-1alpha and beta. J Cell Biochem 110:1226–1233.
Oh JH, Kim A, Park JM, Kim SH, Chung AS. 2006. Ultraviolet B-induced matrix metalloproteinase-1 and -3 secretions are mediated via PTEN/Akt pathway in human dermal fibroblasts. J Cell Physiol 209:775–785.
Park HJ, Costa RH, Lau LF, Tyner AL, Raychaudhuri P. 2008a. Anaphase-promoting complex/cyclosome-CDH1-mediated proteolysis of the forkhead box M1 transcription factor is critical for regulated entry into S phase. Mol Cell Biol 28:5162–5171.
Park HJ, Wang Z, Costa RH, Tyner A, Lau LF, Raychaudhuri P. 2008b. An N-terminal inhibitory domain modulates activity of FoxM1 during cell cycle. Oncogene 27:1696–1704.
Rittie L, Fisher GJ. 2002. UV-light-induced signal cascades and skin aging. Ageing Res Rev 1:705–720.
Rocco JW, Leong CO, Kuperwasser N, DeYoung MP, Ellisen LW. 2006. p63 mediates survival in squamous cell carcinoma by suppression of p73-dependent apoptosis. Cancer cell 9:45–56.
Rodier F, Campisi J. 2011. Four faces of cellular senescence. J Cell Biol 192:547–556.
Rosette C, Karin M. 1996. Ultraviolet light and osmotic stress: Activation of the JNK cascade through multiple growth factor and cytokine receptors. Science 274:1194–1197.
Saygun I, Karacay S, Serdar M, Ural AU, Sencimen M, Kurtis B. 2008. Effects of laser irradiation on the release of basic fibroblast growth factor (bFGF), insulin like growth factor-1 (IGF-1), and receptor of IGF-1 (IGFBP3) from gingival fibroblasts. Lasers Med Sci 23:211–215.
Shefer G, Oron U, Irintchev A, Wernig A, Halevy O. 2001. Skeletal muscle cell activation by low-energy laser irradiation: A role for the MAPK/ERK pathway. J Cell Physiol 187:73–80.
Shefer G, Partridge TA, Heslop L, Gross JG, Oron U, Halevy O. 2002. Low-energy laser irradiation promotes the survival and cell cycle entry of skeletal muscle satellite cells. J Cell Sci 115:1461–1469.
Taniguchi D, Dai P, Hojo T, Yamaoka Y, Kubo T, Takamatsu T. 2009. Low-energy laser irradiation promotes synovial fibroblast proliferation by modulating p15 subcellular localization. Lasers Surg Med 41:232–239.
Teh MT, Wong ST, Neill GW, Ghali LR, Philpott MP, Quinn AG. 2002. FOXM1 is a downstream target of Gli1 in basal cell carcinomas. Cancer Res 62:4773–4780.
Wang X, Kiyokawa H, Dennewitz MB, Costa RH. 2002. The Forkhead Box m1b transcription factor is essential for hepatocyte DNA replication and mitosis during mouse liver regeneration. Proc Natl Acad Sci USA 99:16881–16886.
Wang IC, Chen YJ, Hughes D, Petrovic V, Major ML, Park HJ, Tan Y, Ackerson T, Costa RH. 2005. Forkhead box M1 regulates the transcriptional network of genes essential for mitotic progression and genes encoding the SCF (Skp2-Cks1) ubiquitin ligase. Mol Cell Biol 25:10875–10894.
Wierstra I, Alves J. 2008. Cyclin E/Cdk2, P/CAF, and E1A regulate the transactivation of the c-myc promoter by FOXM1. Biochem Biophys Res Commun 368:107–115.
Wlaschek M, Ma W, Jansen-Durr P, Scharffetter-Kochanek K. 2003. Photoaging as a consequence of natural and therapeutic ultraviolet irradiation–studies on PUVA-induced senescence-like growth arrest of human dermal fibroblasts. Exp Gerontol 38:1265–1270.
Wonsey DR, Follettie MT. 2005. Loss of the forkhead transcription factor FoxM1 causes centrosome amplification and mitotic catastrophe. Cancer Res 65:5181–5189.
Wu CH, van Riggelen J, Yetil A, Fan AC, Bachireddy P, Felsher DW. 2007. Cellular senescence is an important mechanism of tumor regression upon c-Myc inactivation. Proc Natl Acad Sci USA 104:13028–13033.
Yao KM, Sha M, Lu Z, Wong GG. 1997. Molecular analysis of a novel winged helix protein, WIN. Expression pattern, DNA binding property, and alternative splicing within the DNA binding domain. J Biol Chem 272:19827–19836.
Ye H, Kelly TF, Samadani U, Lim L, Rubio S, Overdier DG, Roebuck KA, Costa RH. 1997. Hepatocyte nuclear factor 3/fork head homolog 11 is expressed in proliferating epithelial and mesenchymal cells of embryonic and adult tissues. Mol Cell Biol 17:1626–1641.
Yu HS, Wu CS, Yu CL, Kao YH, Chiou MH. 2003. Helium-neon laser irradiation stimulates migration and proliferation in melanocytes and induces repigmentation in segmental-type vitiligo. J Invest Dermatol 120:56–64.
Zhang J, Xing D, Gao X. 2008. Low-power laser irradiation activates Src tyrosine kinase through reactive oxygen species-mediated signaling pathway. J Cell Physiol 217:518–528.
Zhang L, Xing D, Gao X, Wu S. 2009. Low-power laser irradiation promotes cell proliferation by activating PI3K/Akt pathway. J Cell Physiol 219:553–562.
Zhang L, Zhang Y, Xing D. 2010b. LPLI inhibits apoptosis upstream of Bax translocation via a GSK-3beta-inactivation mechanism. J Cell Physiol 224:218–228.
Zhang H, Wu S, Xing D. 2011. YAP accelerates Abeta(25–35)-induced apoptosis through upregulation of Bax expression by interaction with p73. Apoptosis 16:808–821.
Zhang H, Wu S, Xing D. 2012. Inhibition of Abeta(25–35)-induced cell apoptosis by low-power-laser-irradiation (LPLI) through promoting Akt-dependent YAP cytoplasmic translocation. Cell Signal 24:224–232.
Zhao Q, Chen N, Wang WM, Lu J, Dai BB. 2004. Effect of transforming growth factor-beta on activity of connective tissue growth factor gene promoter in mouse NIH/3T3 fibroblasts. Acta Pharmacol Sin 25:485–489.